bioRxiv preprint doi: https://doi.org/10.1101/504837; this version posted December 25, 2018. The copyright holder for this preprint (which was not certified by peer review) is the author/funder, who has granted bioRxiv a license to display the preprint in perpetuity. It is made available under aCC-BY-ND 4.0 International license.

Resistance to ALK targeting therapies as a gradual Darwinian adaptation to inhibitor specific selective pressures

Robert Vander Velde[1,2], Nara Yoon[3], Viktoriya Marusyk[1], Andrew Dhawan[3], Olena Balynska[1], Bina Desai[1,4], Diego Lozano-Peral[1,5], Daria Myroshnychenko[1], Jan Poleszczuk[6], Liu Kenian[7], Omar Mian[3], Mohamed Abazeed[3], Eric Haura[8], Jacob G. Scott[3*], and Andriy Marusyk[1*]

1 Department of Cancer Physiology, H Lee Moffitt Cancer Centre and Research Institute, Tampa, FL, USA.
2 Department of Molecular Medicine, University of South Florida, Tampa, FL, USA.
3 Department of Translational Hematology and Oncology Research, Cleveland Clinic, Cleveland, OH, USA.
4 University of South Florida Cancer Biology PhD Program, Tampa, FL, USA.
5 University of Málaga, Málaga, Spain
6 Nalecz Institute of Biocybernetics and Biomedical Engineering, Polish Academy of Sciences **7** Department of Pahtology, H Lee Moffitt Cancer Centre and Research Institute, Tampa,FL, USA.
8 Department of Thoracic Oncology, H Lee Moffitt Cancer Centre and Research Institute, Tampa, FL, USA.

***to whom correspondence should be address: Andriy.Marusyk@moffitt.org, scottj10@ccf.org**

Competing interests

The authors declare no competing interests.

Running title

Resistance to ALK targeting therapies as a gradual Darwinian adaptation

Keywords

somatic evolution, evolution of resistance, mathematical model, Darwinian evolution

bioRxiv preprint doi: https://doi.org/10.1101/504837; this version posted December 25, 2018. The copyright holder for this preprint (which was not certified by peer review) is the author/funder, who has granted bioRxiv a license to display the preprint in perpetuity. It is made available under aCC-BY-ND 4.0 International license.

Abstract

Despite high initial efficacy, therapies that target abnormal kinase activities, including those directed against the oncogenic EML4-ALK fusion product, eventually fail in advanced, metastatic cancers. This failure in the initially responsive tumors is the direct result of the evolution of drug resistance under therapy-imposed selective pressures. In contrast to the solid body of research on molecular mechanisms of resistance, our understanding of how resistance evolves remains rudimentary and is primarily based on conjectures rather than direct experimental studies. To overcome this gap of knowledge, we set out to investigate the evolution of resistance to clinical ALK inhibitors in an experimental model of ALK positive NSCLC. We found that different ALK inhibitors select for predictably distinct resistant phenotypes, which originate from heterogeneous weakly resistant (tolerant) subpopulations, and gradually evolve toward strong bona fide resistance. This gradual development of resistance is mediated by the acquisition of multiple cooperating molecular mechanisms, involving both genetic copy number alterations and stable changes in gene expression. Whereas tolerance and resistance to ALK TKIs is not associated with fitness penalty, evolving cells display temporally restricted collateral sensitivity to a dual EGFR/HER2 inhibitor, suggesting a novel angle for therapeutic interference.

Introduction

Despite strong initial tumor responses, inhibitors that target abnormal activities of oncogenic tyrosine kinases (TKIs), including front and second line TKIs directed against EML4-ALK fusion oncogene in non-small cell lung cancers (NSCLC), are rarely curative in advanced disease [1]. ALK targeting TKIs (ALK-TKIs) fail to eradicate all of the tumor cells, enabling the surviving tumor cells to evolve resistance-conferring phenotypic adaptations, culminating in the outgrowth of resistant subpopulations and eventual clinical relapse. However, this evolution under the drug-imposed selective pressures is not accounted for in the current clinical practices, where tumors are treated as static entities, with therapy switched only after tumors start relapsing. On the other hand, explicit consideration of the evolutionary dynamics offers a potential opportunity of drastically improving clinical outcomes with tools that are already at our disposal [2–5]. For example, accounting for frequency dependent selection and fitness tradeoffs provided a theoretical foundation for a pilot clinical trial in castration resistant prostate cancer, which significantly extended progression free survival while reducing side effects of the treatment using different scheduling of standard therapy drugs [6].

Achieving the full potential of evolutionary informed therapies requires adequate understanding of the underlying evolutionary dynamics, captured rigorously in the formalism of mathematical models - an area of knowledge that is currently lagging. In contrast to massive research efforts that have advanced our understanding of molecular mechanisms of resistance, evolutionary dynamics during the acquisition of resistance receives little experimental attention. Consequently, our current understanding how resistance evolves is primarily based on conjectures, rather than direct experimental studies and quantitative models. Demonstrations of pre-existence of therapy-associated molecular alterations in sub-populations of tumor cells within treatment naïve samples has led to the widely prevalent assumption that resistance to targeted therapies is simply due to an expansion of pre-existent genetically (or epigenetically) distinct, therapy-resistant subpopulations under drug-imposed selective pressures [7, 8]. An alternative model posits that therapy resistance can emerge

bioRxiv preprint doi: https://doi.org/10.1101/504837; this version posted December 25, 2018. The copyright holder for this preprint (which was not certified by peer review) is the author/funder, who has granted bioRxiv a license to display the preprint in perpetuity. It is made available under aCC-BY-ND 4.0 International license.

de novo from drug-tolerant (DT) sub-populations [9], which are often equated with cancer stem cells [10]. DT cells are thought to be capable of surviving therapies at the expense of significantly reduced proliferation both in and out of therapies. While DT cells cannot sustain tumor growth in the face of therapy, they can maintain residual disease and serve a substrate for a single-hit mutational or epigenetic conversions to therapy-resistant phenotypes, capable of driving robust growth rates in the face of therapy [9].

Motivated by our interest in developing evolutionary informed therapeutic scheduling to tackle TKI resistance, we decided to investigate the origin, and evolutionary dynamics, underlying the rapid development of therapy resistance in an *in vitro* model of ALK+ NSCLC. We found that, upon exposure to different ALK-TKIs, NIH-H3122 cells rapidly and predictably develop strong drug resistance. Rather than reflecting an expansion of pre-existent resistant subpopulations, resistance originates from heterogeneous pre-existing DT sub-populations which proliferate normally in the absence of the drug, and are capable of survival and slow proliferation under ALK-TKIs. DTs cells progress toward *bona fide* resistance gradually, through acquisition of multiple cooperating resistance-contributing mechanisms. This gradual development of resistance might represent an opportunity for therapeutic intervention to forestall acquisition of strong therapy resistance, as evolving populations reliably display collateral sensitivity to a dual EGFR/HER2 inhibitor lapatinib, which is absent in both treatment naïve and fully resistant cells.

Results

Exposure to distinct ALK-TKI leads to the development of distinct resistant phenotypes

To understand the development of acquired resistance to ALK-TKIs, we took advantage of a well-characterized ALK+ NSCLC cell line H3122, which can rapidly develop resistance to multiple clinically relevant ALK-TKI using dose escalation protocols [11]. Using cell lines from our previous study [11], we continued dose escalation, eventually selecting for cells capable of growing in high, clinically relevant concentrations of the drugs (up to 1 μM Criz, 4 μM Lor, 2 μM Alectinib, 200 nM Ceritinib). H3122 cells with evolved resistance to ALK-TKI (erALK-TKI) displayed strong collateral resistance toward all other tested ALK-TKIs, with 5-100x higher LD50, (Fig. 1A and Table S1). Despite the similar shift in LD50 in all of the tested ALK-TKI, erALK-TKI cells developed through selection by different inhibitors displayed more divergent sensitivities to higher drug concentrations. Consistent with the clinical efficacy of alectinib as a second line therapy after failure of crizotinib, high concentrations of alectinib and lorlatinib strongly inhibited cells with evolved resistance to crizotinib (erCriz) and ceritinib (erCer). The resistance was at least partially heritable, as the erALK-TKI phenotypes were partially or completely maintained after drug holiday (Fig. S1). Further, upon xenograft transplantation into immunocompromised NSG mice, cells with evolved resistance to alectinib (erAlec) and lorlatinib (erLor), formed tumors capable of maintaining net growth when challenged with clinically relevant concentrations of alectinib and lorlatinib, despite the 3 weeks gap between tumor implantation and initiation of the treatment (Fig. 1B, C).

Whereas drug dose escalation protocols are commonly used in studies to identify resistance mechanisms [12], they do not reflect the development of resistance in clinics, as patients are treated upfront with highest tolerated doses of the drugs. Therefore, we asked whether resistance can develop in the face of acute exposure to clinically relevant concentrations of ALK-TKIs. To this end, we plated treatment naïve H3122 cells in the presence of 1 μM (Crizotinib, Alectinib and Lorlatinib) or 100 nM (Ceritinib) ALK-TKI, replating cultures as needed to relieve contact growth

bioRxiv preprint doi: https://doi.org/10.1101/504837; this version posted December 25, 2018. The copyright holder for this preprint (which was not certified by peer review) is the author/funder, who has granted bioRxiv a license to display the preprint in perpetuity. It is made available under aCC-BY-ND 4.0 International license.

inhibition of the surviving cells. After 3-4 months of this selection, we obtained rapidly proliferating erALK-TKIs cell lines, with resistance levels compatible to those achieved with the dose escalation protocol (Fig. 1D).

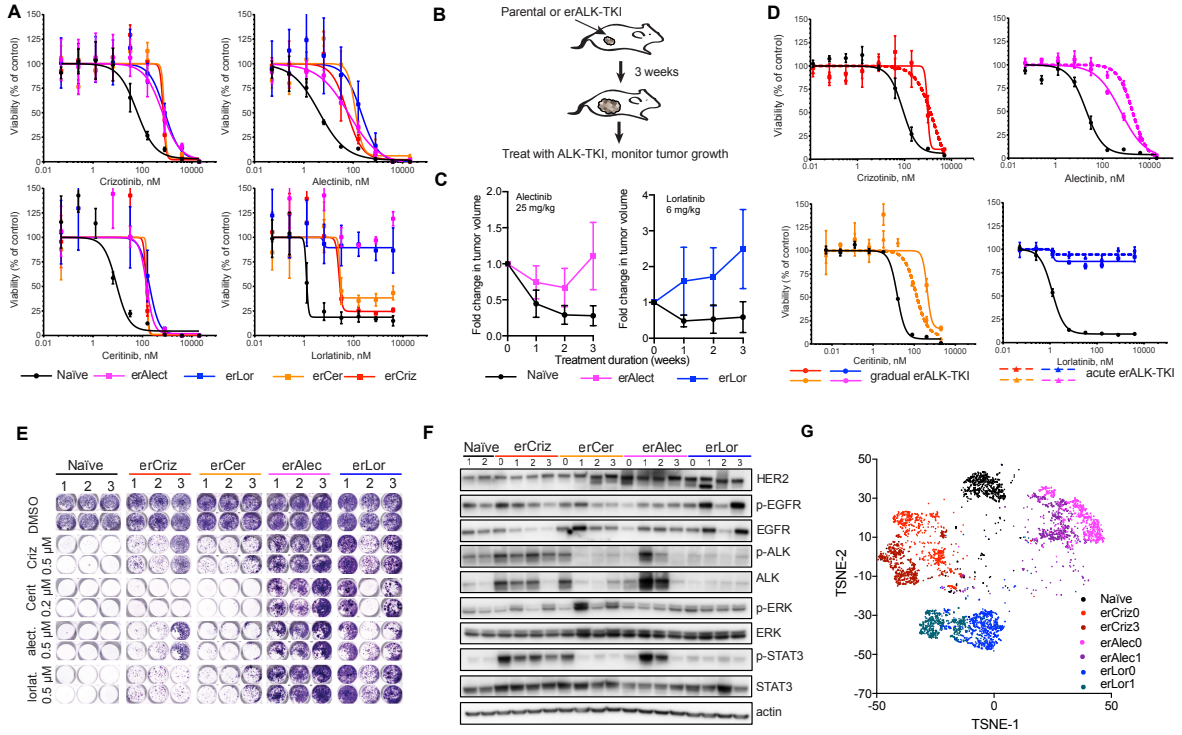

Figure 1. Characterization of evolved resistance to distinct ALK-TKIs. A. Sensitivities of the treatment naïve H3122 cell and indicated erALK-TKI derivative cell lines to the indicated ALK inhibitors, measured by Cell Titer Glo assay. B. Experimental schemata of the xenograft experiment. C. Growth dynamics of xenograft tumors produced by inoculation of the indicated cells. Treatment with indicated concentrations of ALK TKIs or vehicle control is started 3 weeks post implantation. D. Comparison of resistance levels of erALK-TKI cells evolved by gradual and acute drug exposure, measured by Cell Titer Glo assay. E. Sensitivity of independent derivates of erALK-TKI cells to the indicated ALK-TKIs, measured by crystal violet assay. F. Immunoblot analysis of the expression levels of the indicated proteins in the independent derivations of erALK-TKI cells. "0" denotes gradually derived erALK TKI cell lines, presented in Figure A, "1-3" indicates independent derivate sub-lines obtained by acute selection for resistance in high drug concentrations, same as in E. G. tSNE analysis of single cell RNA-seq expression of the indicated cell lines.

We next asked to what extent the differences in cross-sensitivities of erALK-TKI cells towards different ALK inhibitors are attributable to the selection agent. To answer this, we independently derived triplicate lines for each of the ALK-TKIs used in this study with the acute exposure protocol, and compared their cross-sensitivities to higher concentrations of the inhibitors. Consistent with previous findings (Fig. 1A), erLor and erAlec cells demonstrated stronger resistance to high concentrations of different ALK-TKI, compared to erCriz and erCer cell lines (Fig 1E). Similar to the resistant cell lines derived by gradual exposure, resistant phenotypes in cell lines derived by acute exposure to ALK TKIs were largely heritable (FIG S2).

It is frequently assumed that resistance-conferring phenotypes should be associated with strong baseline fitness penalties compared to drug naïve tumor cells. This fitness penalty enables adaptive therapy, which creates an evolutionary "tug of war" between therapy sensitive and therapy naïve populations by sequencing primary drug with strategic treatment breaks, informed by tumor response to the drugs [4]. Thus, we examined growth of erALK-TKI cell lines in the presence and absence of the drugs. Whereas in some cases, cells taken off the drugs indeed proliferated slower than drug

bioRxiv preprint doi: https://doi.org/10.1101/504837; this version posted December 25, 2018. The copyright holder for this preprint (which was not certified by peer review) is the author/funder, who has granted bioRxiv a license to display the preprint in perpetuity. It is made available under aCC-BY-ND 4.0 International license.

naïve control, some of the resistant cell lines proliferated at similar or even higher rates (Fig. S3A). Interestingly, all of the examined erCriz and 1/3 of examined erAlec cell lines displayed higher rates of proliferation in the presence of the inhibitors, consistent with previously reported observations in melanoma [13, 14]; the remaining cell lines were either modestly inhibited, or unaffected by the ALK-TKI used for their selection (Fig. S3A). Inferences obtained from *in vitro* 2d cultures, however, could be misleading. Fitness of tumor cells is context dependent [15, 16], and *in vitro* 2d cultures do not necessarily accurately capture death/proliferation dynamics within tumors *in vivo*. Further, non-cell autonomous interactions between phenotypically distinct subpopulations could significantly alter fitness in competitive settings [17, 18]. Therefore, we tested the fitness impact of resistance conferring adaptations by implanting mixtures of differentially labelled (GFP and mCherry) resistant and naïve cells into subcutaneous tumors or into lungs (via tail vein injections). Only erCriz cells injected to lungs displayed reduced fitness compared to the therapy naïve cells (Fig. S3B). Interestingly, erLor cells displayed a substantial selective advantage over naïve cells both in subcutaneous and orthotopic tumor contexts. These data suggest that resistance to ALK TKI is not necessarily linked with strong fitness advantage, implying that these tumors might be poor candidates for adaptive therapies based on treatment breaks.

Given the surprising predictability in ALK-TKI cross-sensitivity phenotypes, we interrogated the extent of predictability of changes in EML4-ALK dependent signaling pathways. Immunoblot analyses, performed on cells cultured in the absence of the drugs for 48 hrs (to minimize the direct impact of ALK-TKIs on cell signaling) revealed that all of the erCriz cell lines displayed increased phosphorylation of EML4-ALK, in most cases in association with elevated EML4-ALK protein levels, as well as increased activating STAT3 phosphorylation (Fig. 1F). In contrast, all of the erLor cell lines lacked the increase in STAT3 phosphorylation and displayed reduced ALK phosphorylation. Instead, they expressed higher levels of EGFR, HER2, or both. erAlec and erCer cell lines exhibited more diverse (less predictable) phenotypes. To assess the phenotypes more globally, we examined mRNA expression levels of 230 cancer-related genes using Nanostring nCounter GX human cancer reference panel. Principal component and hierarchical clustering analyses for mRNA expression were largely consistent with the immunoblot evaluation of phosphorylation (Fig. S4A, B). erCer, evolved through acute selection, as well as acutely and gradually evolved erCriz and erLor cells formed distinct clusters; in contrast, phenotypes of erAlec were more diverse. In principle, observed differences could reflect either cell population-wide phenotypic changes or differences in relative abundance of distinct pre-existent subpopulations. To discriminate between these two possibilities, we performed single cell RNA sequencing of erALK-TKI cell lines, focusing on two cell lines per group with the highest divergence in PCA analysis of NanoString data (S4A). tSNE analysis of single cell expression data revealed relative phenotypic homogeneity within individual ALK-TKIs lines, with high degree of similarity among cell lines derived with the same inhibitor (Fig 1G). Thus, despite a contribution of stochastic component, the evolution of resistance to ALK-TKIs produces highly predictable phenotypes, with strong divergence between phenotypes selected by different ALK inhibitors.

Resistance to distinct ALK TKI develops from heterogeneous pre-existing sub-populations

Evolution of acquired resistance to targeted therapy is commonly assumed to reflect a simple expansion of therapy resistant sub-populations [19]. To test whether this is the case for the acquired resistance to ALK-TKis, we seeded treatment naïve NCI-H3122 cells at clonogenic densities in the presence of ALK-TKIs or DMSO (vehicle control). At 10 days post seeding, the majority of treat-

bioRxiv preprint doi: https://doi.org/10.1101/504837; this version posted December 25, 2018. The copyright holder for this preprint (which was not certified by peer review) is the author/funder, who has granted bioRxiv a license to display the preprint in perpetuity. It is made available under aCC-BY-ND 4.0 International license.

ment naïve cells plated in DMSO, as well as erALK-TKI cells plated in DMSO or ALK-TKIs, formed macroscopic colonies. In contrast, we could not detect macroscopic colonies upon plating as many as 10,000 treatment naïve in the presence of ALK-TKIs. Instead, we observed large numbers of small colonies (Fig. 2A). At the same time, limiting dilution experiments revealed that 1:338 - 1:660 of treatment naïve NCI-H3122 cells give rise to robustly growing drug-resistant colonies within 10 weeks of drug exposure (Fig. 2B, C), indicating that most, if not all, of the erALK TKI cells originate from DT intermediates, capable of survival but with limited proliferation under the drugs. This inference is consistent with time lapse microscopy examination of the dynamics of emergence of drug resistance, where robust growth in the presence of ALK-TKIs was observed, but only after significant delay (**Suppl. video 1**).

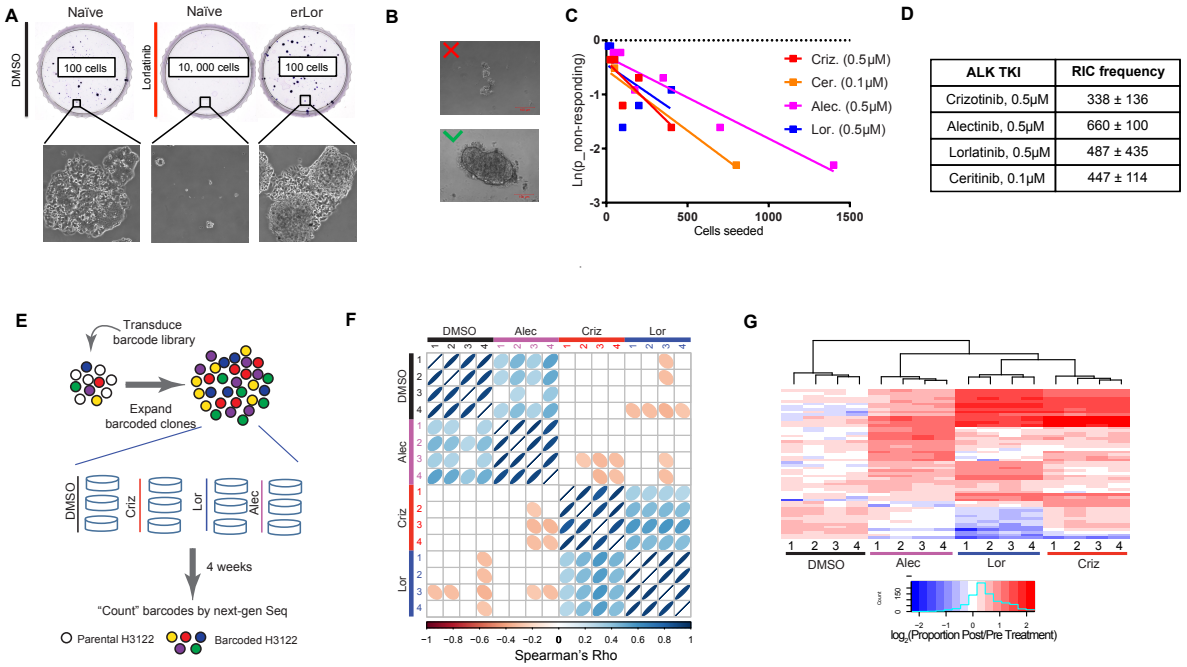

Figure 2. Resistance to ALK TKIs arises from heterogeneous DT sub-populations. A. Representative images of crystal violet stained whole plates and microscopic images of colonies (at 10x magnification) following 10 days of culture. B. Illustration of the size cut-off criteria used for quantitation of limited dilution experiments. C. D, Fitting of limiting dilution assay data and quantitation of frequency of resistance - initiating cells. E. Schemata of the clone tracing experiment. F. Spearman pairwise correlation analysis of barcodes, which have reached frequency, exceeding the highest frequency barcode in the initial cell mix, from the indicated biological replicates. G. Hierarchical clustering analysis of the same "winning" barcodes as in F.

The existence of DT "persisters", as precursors to bona fide resistance has been widely studied in microbiology [20,21]. It has also been documented in EGFR+ NSCLC [9], and other cancers [22–24], and might be a main contributor to minimal residual disease. Potentially, DT cells might either pre-exist prior to therapy, or arise stochastically in response to the drug-induced stress. To discriminate between these two scenarios, we used tracing with selectively neutral DNA barcodes, an approach which has been previously used to demonstrate pre-existence of sub-populations resistant to EGFR inhibitors in EGFR+ lung cancers [25]. We transduced H3122 with a high complexity lentiviral ClonTracer library at low MOI to ensure that most of the transduced cells are labelled with a single unique barcode. Following the elimination of non-transduced cells with puromycin selection, and 100x expansion of the barcoded cells, we took a baseline aliquot, then separated the cells into parallel quadruplicate cultures, and exposed them to 0.5 μM alectinib, lorlatinib, and crizotinib or DMSO control. After 4 weeks of incubation, barcode frequencies were determined by next

bioRxiv preprint doi: https://doi.org/10.1101/504837; this version posted December 25, 2018. The copyright holder for this preprint (which was not certified by peer review) is the author/funder, who has granted bioRxiv a license to display the preprint in perpetuity. It is made available under aCC-BY-ND 4.0 International license.

generation sequencing, and compared to the baseline frequencies (Fig. 2E). Spearman ranking of barcodes, which increased in frequency above the highest barcode frequency observed in the baseline sample, indicated a strikingly high degree of correlation between biological replicates within the same treatment condition, indicating pre-existence of relatively stable DT subpopulations (Fig. 2F). However, correlation between samples treated with different ALK TKI was either absent or much less pronounced, indicating that selective pressures exerted by different ALK TKIs might amplify distinct pre-existing sub-populations. A less stringent hierarchical clustering analysis revealed a partial overlap between "winning" clones (barcodes) across multiple ALK TKIs, indicating that some of the resistant phenotypes provide equally good adaptation to different ALK TKIs (Fig. 2G). In contrast to the fitness cost of classical persistence under the baseline growth conditions [21], clones selected by different ALK-TKIs did not display an obvious fitness penalty in the absence of the drug, as most of them did better than average in the DMSO control (Fig S5). Thus, consistent with recent findings in melanoma [24], resistance to ALK-TKI in H3122 cells originates from pre-existent, heterogeneous subpopulations of DT cells, which display varying sensitivity to distinct ALK-TKIs.

Graduality of the development of ALK-TKI resistance

Having established that resistance originates from heterogeneous pre-existing DT populations, we next asked how drug tolerance progresses toward full resistance. The prevalent assumption in the modeling, experimental and clinical communities is that resistance results from a single, saltational transition mediated by acquisition of a genetic mutation or by (meta) stable change in expression of resistance-conferring genes through an epigenetic switch [7,26]. To test whether resistance in H3122 cells develops through a single hit transition, we employed the following clonogenic assay (Fig. 3A). Therapy naïve cells were pre-cultured in the presence of ALK-TKIs (crizotinib or lorlatinib) for 1-3 weeks, then harvested and seeded at clonogenic densities in the presence or absence of the drug. After 7 days of culture, we measured clonogenic survival as well as the sizes of the resulting colonies. Since prolonged exposure in the drugs is expected to eliminate sensitive populations, while enriching for drug tolerant and resistant ones, we expected the clonogenic proportion to increase over time. Indeed, clonogenic proportion in 0.5 μM crizotinib progressively increased from the initial 2.6% to 26% at week three, while clonogenic proportion in 0.5 μM lorlatinib increased from the initial 1% to 17% at week three (Fig. 3B). If transition from tolerance to resistance were to result from a single-hit mutational or epimutational switch, we would expect to observe a bimodal distribution of colony sizes, representing DT and resistant colonies, with fraction of the latter gradually increasing (Fig. 3A). Consistent with the lack of proliferation penalty in the barcoding experiments, we did not observe substantial changes in size of colonies, formed by cells with evolved or evolving resistance, in the absence of the drugs (Fig S6 A, B). As expected, longer ALK TKI exposure lead to an increase in average colony size. However, instead of the expected bimodal size distribution, this increase was apparently homogeneous, suggesting a gradual development of resistance (Fig. 3C). Analysis of the colony size distributions at the intermediate (2 and 3 weeks) time-points using Kolmogorov-Smirnov statistics revealed that the observed colony sizes cannot be explained by mixing from the distribution of colony size distributions of treatment naïve and erALK-TKI cells (Fig. S6 C, D).

Inferences with Kolmogorov-Smirnov statistics might be obfuscated by the fact that (epi)mutations mediating transition from tolerance to *bona fide* resistance can potentially occur not only during the 1-3 weeks growth preceding the clonogenic assay, but also during this assay. Therefore, to discriminate between a single step and multi-step development of resistance, we developed an agent based mathematical model of the evolution of therapy resistance, which enabled *in silico* simulation of the

bioRxiv preprint doi: https://doi.org/10.1101/504837; this version posted December 25, 2018. The copyright holder for this preprint (which was not certified by peer review) is the author/funder, who has granted bioRxiv a license to display the preprint in perpetuity. It is made available under aCC-BY-ND 4.0 International license.

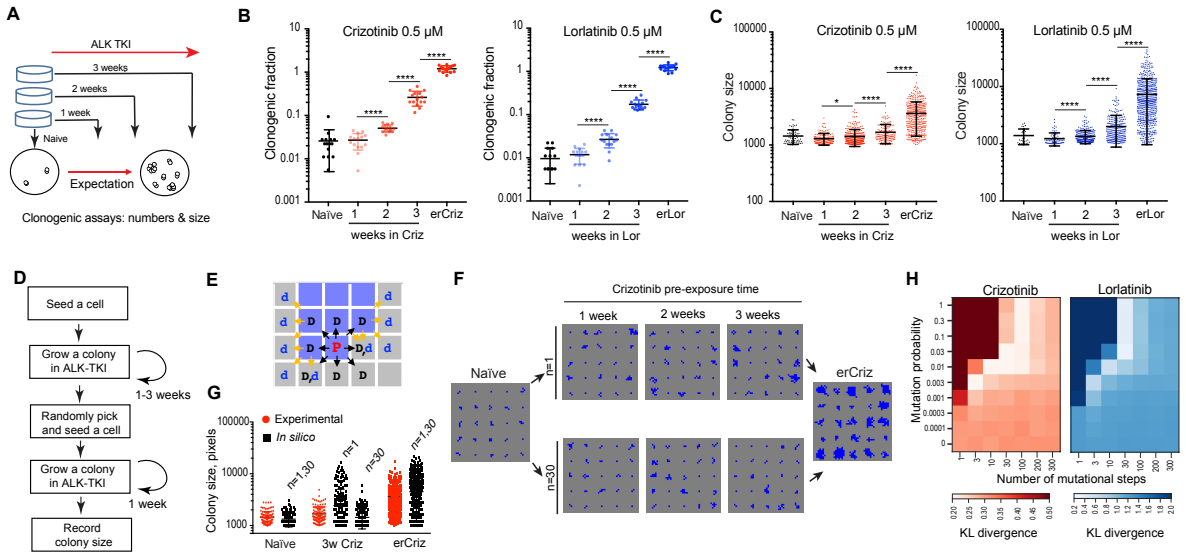

Figure 3. Gradual development of acquired ALK TKI resistance. A. Schemata for of the experiment to assess the mode of progression from tolerance to resistance. B. Clonogenic survival in the presence of the drug after pre-incubation for indicated times in crizotinib and lorlatinib; data is normalized to clonogenic survival in DMSO control. C. Colony sizes distribution of the colonies in the presence of the indicated ALK TKI. * and **** represent p values of Mann-Whitney non-parametric test, < 0.05 and < 0.0001 respectively. D. Logical flow diagram for the agent-based mathematical model. The model simulates growth from initial seeding through pre-incubation and the clonogenic assay. E. Proliferation space check scheme. Blue and green cells denote occupied and empty spaces respectively. "P" stands for the parental cell, "D" for daughter cell, "d" for displaced cell. Black arrow indicates options for movement of daughter cells, yellow arrows - for displaced cells. F. Example of simulations of colony growth, initiated from cells pre-incubated in crizotinib for the indicated period of time, during the final colony assay, contrasting $n = 1$ versus $n = 30$. G. Comparing divergence between *in silico* and experimental data, with $n = 1$ and 30. H. Kullback–Leibler divergence-based comparison of the experimental data with the outcomes of simulations, covering parameter space for the indicated mutation probabilities and numbers of mutational steps.

experimental assay across a range of mutational probabilities and numbers of mutational steps (Fig. 3D, Mathematical Supplement). This model simulates growth of individually seeded cells and their progeny in the presence/absence of the drug both prior and during the clonogenic assay. Cells are seeded into a 2d lattice (simulating the surface of culture dish). If space is available (no more than one cell separating the cell from an empty space), a cell can proliferate with a given probability inferred from the experimental data (Fig. 3E). To account for the variability of the observed colony sizes, the maximal proliferation probability is set for each simulated colony individually, based on random sampling of colony sizes of colonies produced by resistant cells. For the initial proliferation probability, we use one single value calibrated with the whole distribution of naïve cell colony sizes, assuming minor variability in the proliferation rates of such cells. At each cell division, a cell can increase a division rate, reflecting adaptive (epi-)mutations. Cells can transition from the initial to maximal division probability by either a single step ($n = 1$), or multiple ($n > 1$) steps, representing fractional increments of the single transition (Fig. 3D and Mathematical Supplement). Whereas the initial and maximal growth rates are fixed based on the experimental data, the intermediate rates within *in silico* simulations are not. They can differ based on two parameters: a) (epi) mutational probability and b) the number of mutational steps required to reach maximum division probability (n). Since we do not know the (epi) mutation probability, we explored the outcomes with the full range (0-1), and the number of mutational steps ranging from 1 to 300. With each choice of the parameters within the ranges, we generated 100,000 random *in silico* simulations (Fig. 3F and **Suppl. video 2**), and differences between *in vitro* and *in silico* colony size distributions were assessed using the Kullback-Leibler divergence. We found that a single mutational step provided the

bioRxiv preprint doi: https://doi.org/10.1101/504837; this version posted December 25, 2018. The copyright holder for this preprint (which was not certified by peer review) is the author/funder, who has granted bioRxiv a license to display the preprint in perpetuity. It is made available under aCC-BY-ND 4.0 International license.

poorest fit to the data for all of the mutation probabilities. The best fit was achieved with a number of mutational steps in the range of 3-100 (Fig. 3G, H). Therefore, the experimentally observed dynamics of the development of ALK TKI resistance is consistent with a gradual development of resistance, driven by selection for incremental improvements for increased drug resistance, rather than a single (epi) mutational switch.

Molecular mechanisms of resistance to ALK-TKI

Next, we decided to interrogate the molecular mechanisms underlying the evolution of resistance. Clinical resistance to ALK inhibitors is frequently associated with point mutations in the kinase domain of ALK, which reduce drug binding [27]. However, hotspot mutations were absent in the erALK-TKI cell lines, as revealed by targeted Sanger sequencing of PCR-amplified cDNA (Fig. S7). Given that clinical ALK TKI resistance is often associated with EML4-ALK amplification, and the observed increase in the expression of EML4-ALK in some of the erALK-TKI resistant cell lines (Fig. 1F), we tested the amplification status of EML4-ALK in treatment naïve, as well as in representative erALK TKI resistant cell lines (lines "0" in Fig. 1F) using ALK break apart FISH probe test. The majority of the treatment-naïve H3122 cells displayed 4 copies of the WT ALK allele and one copy of the EML4-ALK fusion allele, with a minor sub-population lacking the fusion gene signal. Some of the erALK-TKI cells displayed multiple copies of the fusion allele, consistent with gene amplification (Fig. 4A). Extrachromosomal amplification of oncogene-containing DNA has been recently implicated in rapid evolution of TKI resistance [28], however examination of metaphase spreads revealed that the amplified alleles were still localized within the original translocation region in chromosome 2. Consistent with the immunoblotting results shown in Fig. 1F, we observed substantial heterogeneity in amplification status of EML4-ALK, both between and within erALK-TKI cell lines (Fig. 4B). The majority of erCriz cells, as well as a fraction of erAlec and erCer cells displayed EML4-ALK amplification. In contrast, erLor cells not only lacked EML4-ALK amplification, but also the proportion of oncogene negative cells was significantly lower ($p < 0.0001$ in Chi square test) than in the treatment naïve cells, suggesting that loss of EML4-ALK might have been selectively advantageous.

We next investigated whether differences in EML4-ALK copy numbers corresponded to differences in the oncogene dependence. We transfected treatment naïve, erCriz and erLor cells with constructs expressing CAS9 and two different guide RNA targeting ALK, and selected for puromycin resistant colonies. No colonies could be observed for erCriz cells, suggesting critical dependency on EML4-ALK (Fig. 4C). Parental cells formed few small colonies, resembling tolerant colonies formed upon exposure with ALK-TKI (Fig. 1D). In contrast, erLor cells formed multiple colonies that displayed no evidence of growth inhibition (Fig. 4C), despite complete ablation of the protein expression of EML4-ALK gene (Fig. 4D). Interestingly, puromycin resistant naïve cells transfected with guide RNA directed against ALK displayed lack of EML4-ALK ablation, consistent with strong selection for variants that uncouple antibiotic resistance from guide RNA expression, indicating a strong selective disadvantage of losing expression of EML4-ALK. This observation is consistent with reduced baseline expression of the gene observed in erLor cells (Fig. 1F), and indicates conversion into a phenotype that is independent of EML4-ALK oncogenic activity.

Given that EML4 amplification and overexpression is considered to represent *bona fide* therapy resistance mechanism [29], we asked whether the observed increase in EML4-ALK expression could explain the resistance observed in the erALK-TKI cell lines with EML4-ALK amplification. Retroviral overexpression resulted in protein levels of total and phoshorylated EML4-ALK, which closely resemble those observed in EML4-ALK amplified erALK-TKI cells (Fig. 4E). Further, cells

bioRxiv preprint doi: https://doi.org/10.1101/504837; this version posted December 25, 2018. The copyright holder for this preprint (which was not certified by peer review) is the author/funder, who has granted bioRxiv a license to display the preprint in perpetuity. It is made available under aCC-BY-ND 4.0 International license.

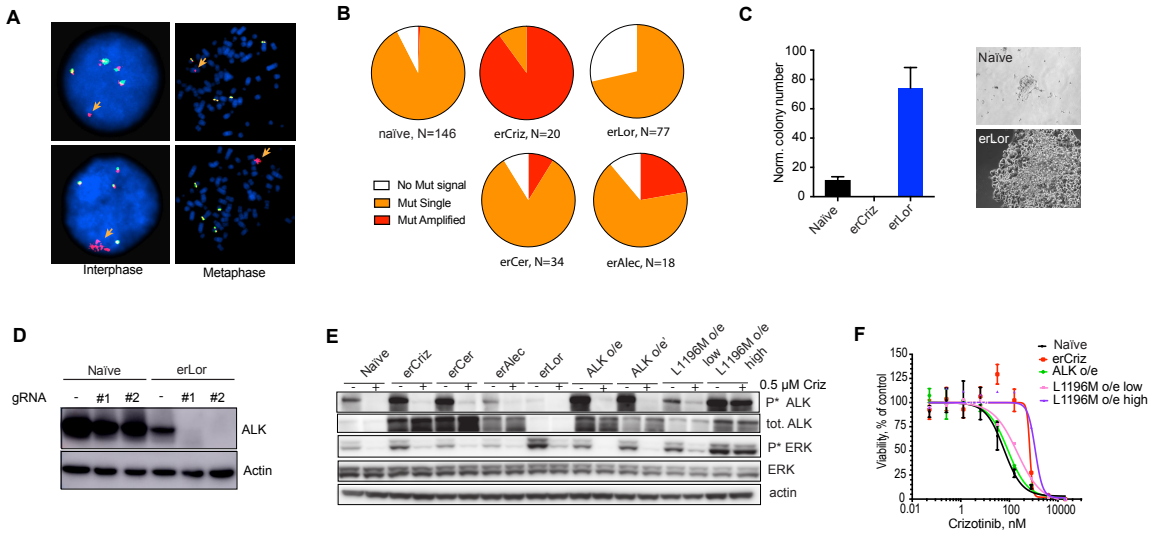

Figure 4. Contribution of ALK expression changes to erALK-TKI phenotypes. A. Representative images for interphase and metaphase FISH analysis for EML4-ALK fusions and amplification status. WT ALK alleles contain signals from both 5' (green) and 3' (red) probes. Single red signal indicates EML4-ALK fusion (orange arrows). B. Frequency of cells with the indicated EML4-ALK fusion and amplification status in the gradually evolved erALK-TKI cell lines. C. Impact of CRISPR mediated genetic ablation of ALK on clonogenic survival of the indicated H3122 derivates. D. Evaluation of EML-ALK ablation status by immunoblotting analysis. E. Immunoblot evaluation of the expression and activity of EML4-ALK oncogenic signaling in the indicated evolved and engineered resistance cell lines. F. Impact of retrovirally mediated overexpression of "wild type" EML4-ALK and its L1196M mutant variant on sensitivity to crizotinib, measured by Cell Titer Glo assay.

with retrovirally overexpressed EML4-ALK retained residual levels of ALK phosphorylation similar to those observed in the erALK-TKI cells (Fig. S8A). Despite this, EML4-ALK overexpressing cells displayed only a marginal increase in ALK TKI resistance (Fig. 4G), suggesting that while ALK amplification contributes to resistance, it is insufficient to fully account for it.

Given the insufficiency of EML4-ALK overexpression to fully account for resistance, we decided to interrogate the functional impact of the most common resistance-associated point mutation, L1196M, which is thought to provide a single hit resistance mechanism [29]. Surprisingly, at low expression levels, achieved with < 1 retroviral MOI, L1196M expression only moderately decreased Crizotinib sensitivity (Fig. 4G). In contrast, higher overexpression of the mutant protein, at levels similar to those observed with cells containing amplified "wild type" fusion gene, blocked the ability of Crizotinib to shut down phosphorylation of EML4-ALK, as well as its main downstream effector ERK (Fig. 4E, S8A, B), and provided resistance level that is similar or higher of that observed in erCriz cells (Fig. 4F). Whereas the results with L1196M overexpression are consistent with previously reported sufficiency to confer resistance in NIH-H3122 cells [30, 31], and ALK mutations do co-occur with EML4-ALK amplification [32], we are not aware of reports of amplification of ALK mutant alleles. Thus, common resistance-associated mutational changes might be insufficient to provide a single hit solution to the challenge posed by ALK TKI induced selective pressures.

Since ALK amplification is insufficient to fully account for the resistant phenotypes of erALK-TKI cell lines, and the Oncomine Focus Assay [33] failed to detect additional common mutational and copy number changes (data not shown), we examined non-genetic mechanisms – probing for stable changes in gene expression, with RNA–Seq analysis of erALK-TKI cells after a 48 hr drug holiday (to reduce to the direct impact of ALK TKI on gene expression). We found multiple gene expression changes, previously implicated in TKI and chemotherapy resistance, including multiple RTKs (EGFR, HER2, FGFR, AXL, EPHA2, etc.), cytokines, ECM & ECM receptors and other types

bioRxiv preprint doi: https://doi.org/10.1101/504837; this version posted December 25, 2018. The copyright holder for this preprint (which was not certified by peer review) is the author/funder, who has granted bioRxiv a license to display the preprint in perpetuity. It is made available under aCC-BY-ND 4.0 International license.

of molecules, suggesting a complex, multifactorial nature of resistance (Fig. 5A). Importantly, co-expression analysis of CCLE cell lines database revealed that the genes with upregulated expression in erALK-TKI cells belonged to distinct gene co-expression clusters, suggesting that the resistance-associated changes in gene expression are unlikely to represent a single coordinated transcriptional program switch (Fig. S9).

Figure 5

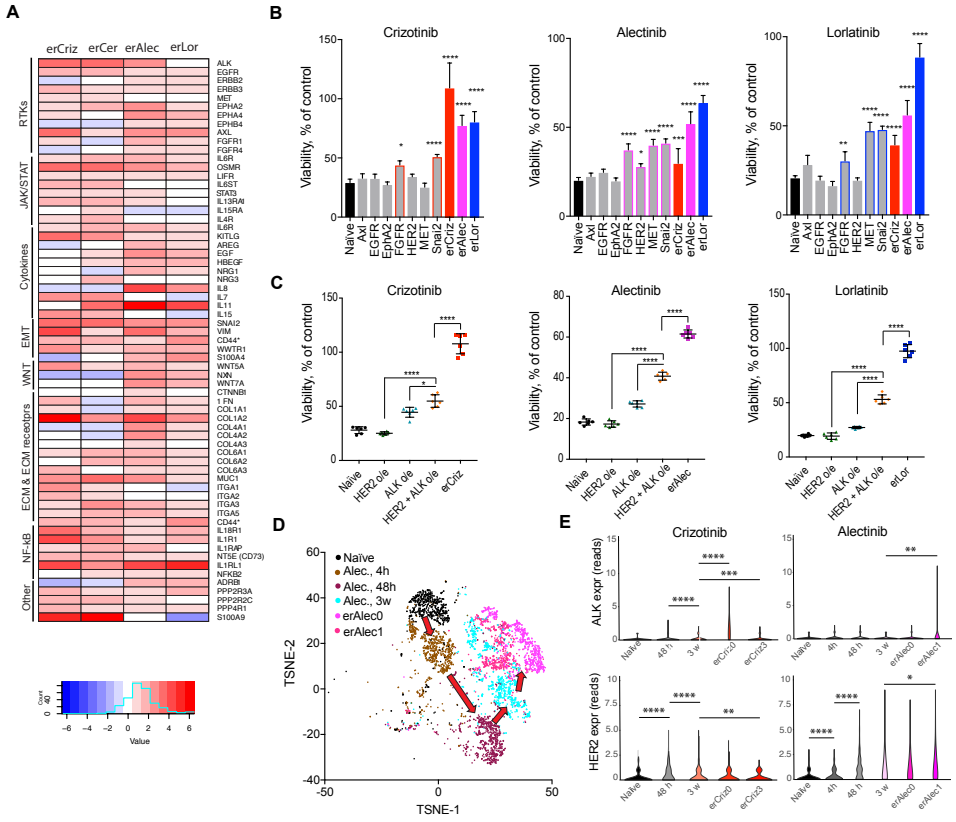

Figure 5. Evolved resistance to ALK TKI integrates multiple mechanisms. A. Elevated mRNA expression for the indicated genes, previously associated with chemotherapy or targeted therapy resistance, in erALK-TKI cell lines across the indicated functional categories. B. ALK-TKI sensitivity of engineered cell lines overexpressing individual putative resistance associated expression changes to the indicated ALK-TKIs (0.5 μM), determined by Cell Titer Glo assay. C. Impact of combination of individual resistance mechanisms toward sensitivity to indicated ALK-TKIs 0.5 μM), determined by Cell Titer Glo assay. *, **, ***, **** represent $p < 0.05$, $p < 0.01$, $p < 0.001$ and $p < 0.0001$ respectively of ANOVA analysis with Dunnett's (B) or Tukey's (C) multiple comparison correction. D. tSNE analysis of single cell mRNA expression data from cells exposed to 0.5 μM alectinib for the indicated time duration. Arrow indicate phenotypic transitions through tSNE space. E. Violin plot of expression levels of ALK and HER2 following indicated duration of exposure to the indicated ALK-TKIs.

To evaluate the functional significance of elevated expression of the resistance-associated genes on ALK-TKI sensitivity, we tested the impact of overexpression of selected genes, previously implicated in TKI resistance. We found that lentiviral overexpression of HER2, FGFR, AXL, and SLUG significantly increased resistance to multiple ALK-TKIs (Fig. 5B). However, resistance levels observed in these engineered cell lines fell short of levels observed in the erALK-TKI lines, suggesting that evolved resistance might reflect the combined effect of multiple contributing changes. To directly evaluate this possibility, we interrogated the impact of the combination of individual genetic and transcriptional changes. We combined overexpression of EML4-ALK, which is amplified in many

bioRxiv preprint doi: https://doi.org/10.1101/504837; this version posted December 25, 2018. The copyright holder for this preprint (which was not certified by peer review) is the author/funder, who has granted bioRxiv a license to display the preprint in perpetuity. It is made available under aCC-BY-ND 4.0 International license.

resistant cell lines (Fig. 1F) and provides a very modest decrease in crizotinib sensitivity (Fig. 4F), with expression of HER2, which is also elevated in multiple erALK-TKI cell lines (Fig. 1F) and can slightly decrease sensitivity to ALK inhibitors, when overexpressed (Fig. 5B). Whereas HER2 overexpression had very limited impact on ALK-TKI sensitivity, it significantly increased resistance conferred by EML4-ALK overexpression, though still falling recapitulate resistance levels observed in erALK-TKI cells (Fig. 5C). These results support the notion that evolution of resistance proceeds through acquisition of multiple genetic and epigenetic changes, that, under inhibitor-specific selective pressures of ALK-TKIs, shape resistant phenotypes in combinatorial fashion.

To gain further insights on the dynamics of phenotypic changes during the evolution of resistance, we analyzed phenotypic changes following different exposure time to ALK TKIs using single cell expression profiling. Consistent with the results reported above, tSNE analysis revealed gradual phenotypic progression from naïve to resistant phenotype (Fig. 5D, S10). Notably, even brief (4 hours) alectinib exposure substantially impacted cell phenotypes, indicating that evolution of resistance reflects not only action of drug-imposed selection, but also direct drug-induced cell adaptation. To get further insight on the temporal dynamics of acquisition of resistance-conferring expression changes, we analyzed the expression of ALK and HER2 at a single cell levels at different time points after exposure to alectinib. Consistent with high levels of ALK expression and genetic amplification of EML4-ALK in erCriz cell lines, expression of ALK gradually increased upon exposure to crizotinib, but not alectinib. In contrast, expression of HER2 became elevated within 48 hours of exposure to both drugs, suggesting direct adaptive response, then decreased upon prolonged incubation with crizotinib, while staying up-regulated or increasing further under alectinib (Fig. 5E).

To explore a possible epigenetic mechanism underlying the observed early and heritable changes in gene expression associated with ALK-TKI exposure, we analyzed the global repatterning of Histone 3.3 lysine 27 acetylation (H3K27ac), a post translational histone modification associated with strong enhancer elements. We performed CHIP-Seq analysis to characterize differential H3K27ac distribution at gene regulatory elements in naïve and evolved resistant lines. We found that different ALK-TKI resistant phenotypes are associated with distinct global patterns of H3K27 acetylation (Fig. S11A). Furthermore, we found variable H3K27ac peaks in putative upstream regulatory enhancer regions associated with genes upregulated in individual ALK-TKI treated lines, e.g. ERBB2 / HER2 (Fig. S11B). Consistent with the differences in protein expression (Fig. 1F) the new peaks were observed in erAlec and erLor lines, but not in the erCriz lines. Taken together, these data suggest that stable gene expression changes might be established and maintained by epigenetic modifications leading to phenotypic stability of otherwise genetically identical but phenotypically distinct lineages.

Evolving resistance is associated with temporally restricted collateral sensitivities

Given the fast dynamics of elevated expression of HER2, and previous implication of rapid up-regulation of non-targeted RTKs in response to TKI-targeted therapies, we have asked whether pharmacological inhibition of HER2 could impact the development of resistance. Indeed, whereas dual EGFR/HER2 inhibitor lapatinib did not impact growth of drug naïve cells, it strongly inhibited development of resistance to alectinib in the combined setting (Fig. S12A). However, despite elevated expression of HER2, erAlec cell lines were not sensitive to lapatinib as a single agent, or in combination with lapatinib, consistent with multifactorial nature of resistant phenotypes (Fig. S12B). Strikingly, intermediate stages of resistance were highly sensitive to lapatinib even as a single agent (Fig. 6A, S12C), suggesting that resistance intermediates might represent a unique therapeutic target (Fig. 6B).

bioRxiv preprint doi: https://doi.org/10.1101/504837; this version posted December 25, 2018. The copyright holder for this preprint (which was not certified by peer review) is the author/funder, who has granted bioRxiv a license to display the preprint in perpetuity. It is made available under aCC-BY-ND 4.0 International license.

Figure 6

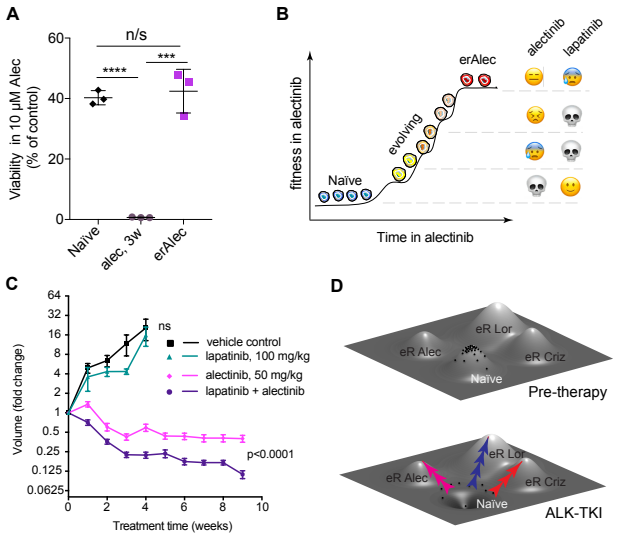

Figure 6. Gradual evolution of resistance provides a new therapeutic window for collateral sensitivity. A. Differential lapatinib sensitivity of naïve, tolerant and erAlec cells, measured by Cell Titer Glo assay. B. Scheme: evolving resistance to alectinib presents an opportunity for therapeutic interference with lapatinib. C. Change in volume of H3122 xenograft tumors treated with indicated therapies; treatment initiated 3 weeks post tumor implantation. **** represents $p < 0.001$ of interaction term of repeated measurements 2-way ANOVA test. D. Evolving resistance interpreted with fitness landscape metaphor. Naïve cells occupy a local fitness peak. Drug exposure reshapes the landscape, turning fitness peak to fitness trough. Different ALK inhibitors act on partially distinct outliers, leading their evolution toward distinct fitness peaks.

Next, we asked whether this collateral sensitivity could be used to improve the efficiency of alectinib therapy. To this end, we inoculated therapy naïve H3122 cells into xenograft mice, allowed them to form tumors for 3 weeks (reaching average volume of 580 mm^3), at which point we initiated a treatment with alectinib, lapatinib, alectinib plus lapatinib combination or vehicle control. Consistent with the *in vitro* data, lapatinib did not impact growth of tumors as a single agent, but significantly increased the efficiency of alectinib therapy when used in combination. Therefore, temporally restricted collateral vulnerabilities of cells evolving resistance to alectinib might be exploited therapeutically to improve depth of responses, and potentially, to forestall the emergence of resistance.

Discussion

In contrast to the ever deepening understanding of proximal molecular mechanisms of resistance, knowledge of its evolutionary causes and dynamics is very limited, and is based primarily on conjec-

bioRxiv preprint doi: https://doi.org/10.1101/504837; this version posted December 25, 2018. The copyright holder for this preprint (which was not certified by peer review) is the author/funder, who has granted bioRxiv a license to display the preprint in perpetuity. It is made available under aCC-BY-ND 4.0 International license.

tures based on single time point observations and assumptions of single hit resistance mechanisms. Therapy resistance is assumed to result from either a selective expansion of pre-existing subpopulation of resistant cells, or from *de-novo* conversion of therapy tolerant persisters into *bona fide* resistant types by either single hit genetic mutation or epigenetic switching/reprogramming. Our work suggests a third, distinct path to resistance, which is identical to the Darwinian postulate of graduality of evolution under natural selection. Rather than reflecting a simple expansion of pre-existent resistant types, or saltational conversion from a well-defined DT sub-population, our study indicates that resistance can originate from heterogeneous, weakly resistant subpopulations. These subpopulations serve as a substrate for drug-specific selective pressures, which drive their gradual adaptation through acquisition of both genetic and non-genetic mechanisms, which cooperatively mediate increased fitness in the presence of the drugs (Fig. 6D).

The Darwinian paradigm, i.e., evolution by natural selection, acting on diverse phenotypes within a population, is a cornerstone of modern biology. It provides an unprecedented power to explain the ability of populations to adapt to environmental changes across the kingdoms of life. Likewise, Darwinian evolution is commonly evoked to explain somatic evolution underlying cancer progression and acquisition of therapy resistance, becoming text-book dogma [34]. On the other hand, within cancer biology, somatic evolution is commonly thought to be a stepwise or branching process of genetic changes, where acquisition of "driving" mutations is both necessary and sufficient to account for the observed phenotypic changes [34–36], which is conceptually much closer to the saltationalist ideas of prominent geneticists prior to evolutionary synthesis, then either Darwin's original postulates or post-synthesis concensus [37]. Complicating things further, while genetic mutations constitute the major engine of diversification in the evolution of natural populations, cancer cells have access to additional powerful, and more plastic sources of diversity operating on different timescales [38]. These include chromosomal instability [36], extrachromosomal genetic inheritance [28], and epigenetic plasticity, which can allow cancer cells to reach distinct stable phenotypic states [39] in the absence of genetic mutations. A growing body of evidence suggest that these additional sources of diversification might be responsible for a large proportion of resistance-conferring phenotypic adaptations [40]. Likewise, acquisition of metastatic potential by pancreatic cancers has been linked to stable epigenetic changes [41]. Within targetable cancer subtypes, where genetic mutations have been strongly implicated, such as resistance to EGFR and ALK inhibitors in lung cancers, a significant proportion of relapsing tumors lacks identifiable resistance-associated mutations [29], suggesting non-mutational causes. Even when a genetic "driver" of resistance can be identified, it might be insufficient to fully explain the resistant phenotypes, as suggested by our overexpression studies with the original EML4-ALK fusion protein, and its commonly mutated version L1196M. Interestingly, a recent single cell sequencing study in triple negative breast cancer demonstrated that while resistance to chemotherapy can be traced to preexistent genetically distinct subpopulations, phenotypic characterization of samples pre- and post-therapy revealed that resistance is associated with acquisition of novel phenotypic changes, which are not associated with new mutations, indicating evolution through non-genetic means [42].

Owing to the dominance of the mutation-centric paradigm in the field of somatic evolution and much higher plasticity compared to small scale genetic mutations, integrating non-genetic sources of phenotypic heterogeneity into the post evolutionary synthesis Darwinian paradigm has been challenging [43]. One approach is to consider heritable epigenetic changes (such as hypomethylation of the CDKN2A locus) as "epimutation" [15]. While resolving the potential conflict with genetic-centric views, the utility of "epimutation" concept as functionally synonymous with genetic mutation is limited - as epigenetic changes usually affect large portions of the genomes (compared to nucleotide changes and small-scale deletions/amplifications) [39] and display a range of heritability [44]. Fur-

bioRxiv preprint doi: https://doi.org/10.1101/504837; this version posted December 25, 2018. The copyright holder for this preprint (which was not certified by peer review) is the author/funder, who has granted bioRxiv a license to display the preprint in perpetuity. It is made available under aCC-BY-ND 4.0 International license.

ther, epigenetic changes are commonly triggered by microenvironmental niches and therapies [45]. Thus, a more common approach to consider resistance-associated (semi)stable epigenetic changes is through the terms of "reprogramming", "epigenetic switch" or "rewiring" [9, 23, 45, 46]. Since somatic evolution is commonly viewed as purely genetic process, identification of epigenetic resistance mechanisms frequently triggers the rejection of Darwinian evolution as an explanation [43]. However, we consider this a false dichotomy, as consideration of resistance associated phenotypic changes as phenotypic transitions within epigenetic landscape needs not to be mutually exclusive of simultaneous selective pressure driven transitions within adaptive landscape [44]. While we have interpreted our findings from the fitness landscape perspective (Fig. 6D), our study, as well as growing body of evidence, (including a recent study in melanoma that describe essentially similar phenomena, while rejecting Darwinian explanation [43]), calls for a post-modern synthesis of Waddington epigenetic and Wright's adaptive landscapes in order to adequately understand somatic evolution.

Coupled with the formidable mechanistic knowledge gained heretofore, adequate understanding of the forces that shape somatic evolution during the acquisition of drug resistance could open the way to application of evolutionary - informed therapy, focused on staying a step ahead of resistance, rather than just reacting to it when it (inevitably) arises. Our data suggest that intermediate stages during the evolution of drug resistance may represent temporally restricted targets for drugs exhibiting collateral sensitivity, paralleling previously reported existence of collateral sensitivities of mutational intermediates of resistance reported for Ph+ ALL [3].

Methods

Derivation of Resistant Cell Lines

Parental and ALK TKI resistant H3122 cells were grown in RPMI (Gibco, Thermo Fisher) supplemented with 10% FBS (Serum Source), penicillin/streptomycin, insulin (Gibco) and anti-clumping agent (Gibco). ALK-TKI resistant cell lines were generated by further evolving lines used in [11], derived through a progressive increase in ALK TKI concentrations, until reaching ability to grow in 0.5 μM crizotinib, 0.2 μM ceritinib, 2.0 μM alectinib and 2.0 μM lorlatinib. Alternatively, resistant lines were derived by exposing treatment naïve H3122 cells directly to the high ALK TKI concentrations, mentioned above, for 3-4 months, with re-plating every 2-4 weeks to relieve spatial growth constraints.

Short Term Viability Assays

Short term cell viability was measured using Cell-Titer Glo reagent (Promega). Typically, 2000 cells per well were plated in a 96-well plate (Costar). Drugs were added 24h later, and the assays were performed using manufacturer recommended protocol 3-4 days after drug addition. Viability was calculated first by subtracting the luminescence of empty wells then by division by average DMSO luminescence. Dose response curves were generated by fitting the following equation to the data:

$$y = b + \frac{100 - b}{1 + \left(\frac{x}{\mathrm{IC}_{50}}\right)^{k}}$$

where y is luminescence, x is drug concentration, IC_{50} is the half maximal inhibitory concentration, k is the hill slope and b is the luminescence as the drug concentration approaches ∞.

bioRxiv preprint doi: https://doi.org/10.1101/504837; this version posted December 25, 2018. The copyright holder for this preprint (which was not certified by peer review) is the author/funder, who has granted bioRxiv a license to display the preprint in perpetuity. It is made available under aCC-BY-ND 4.0 International license.

Clonogenic assays

Cells were plated in the presence of ALK-TKIs or DMSO vehicle control at varying density into 6 cm dishes or multi-well plates in duplicates or triplicates, and grown for 10 days, at which points they were fixed and stained with crystal violet, following protocols described in [47]. To measure the evolution of growth rates, nuclear mCherry expressing H3122 cells were plated at 400,000 cells per 6cm dish, allowed to attach overnight, and exposed to DMSO vehicle control, 0.5 μM lorlatinib, or 0.5 μM crizotinib the following day. After culturing for 1-3 weeks, cells were harvested and seeded at 96-well plates (Costar) at 50 cells/well for DMSO control, or 500 cells for crizotinib and lorlatinib. The number of colonies and colony sizes were measured 1 week later for colonies larger than 1000 pixels (> 5 cells), based on fluorescent area. To minimize the impact of variability in seeding numbers, clonogenic survival in the presence of ALK inhibitors was normalized to clonogenic data in the DMSO controls.

Determining frequency of resistance initiating cells

Cells were plated with initial seeding densities of 400, 400, 800, 1400 and 400 cells/well in DMSO (0.1%), crizotinib (0.5 μM), ceritinib (0.1 μM), alectinib (0.5 μM) and lorlatinib (0.5 μM) treated plates respectively, in a 96-well plate (Falcon). Five additional 2x dilutions (were generated from these wells, each with 10 separate wells. ALK inhibitors were added after 24h. After 7 weeks of treatment, wells containing no colonies larger than 50 cells were counted. The natural log of this number was fitted linearly against the initial cell number in each well. The number of cells per resistance - initiating cell was calculated as $\frac{1}{1-e^{\text{slope}}}$ and the error of this value as $\frac{\text{error}_{\text{slope}} e^{\text{slope}}}{(1-e^{\text{slope}})^2}$.

Clone Tracing Assay

H3122 cells were transduced at 10% efficiency (as defined by FACS analysis of dsRed expression) with ClonTracer neutral DNA barcode library [25], kindly provided by Frank Stegmeyer (Addgene #67267). Barcode containing cells were selected with puromycin and expanded for 23 days. Cells were expanded from 10^5 cells (after puromycin selection) to 3.4×10^7 cells. Quadruplicate cultures of 1.5×10^6 cells each were plated into 10cm dishes in the presence of 0.1% DMSO, 0.5 μM crizotinib, 0.5 μM alectinib and 0.5 μM lorlatinib. Two pellets of 1.5×10^6 cells were frozen to serve as an initial mixture. Cells were harvested following four weeks of cell culture. Genomic DNA was extracted using proteinase K digest, followed by phenol-chloroform purification. Barcodes were amplified, sequenced and analyzed following protocols described in [25] and updated procedures provided at Addgene website `https://www.addgene.org/pooled-library/clontracer`. First round of amplifications was performed for 35 cycles using the following primers TCG ATT AGT GAA CGG ATC TCG ACG and AAG TGG ATC TCT GCT GTC CCT G for 35 cycles. Second round was performed for 15 cycles. All analysis was performed on barcodes that had a higher proportion than the barcode with the highest proportion in the pretreatment group, in at least one other group. Heatmap.2 in R (using default parameters) was used for heatmap clustering. Corrplot [48] in R (using Spearman correlation coefficients) was used to visualize correlations.

Fluorescent In situ Hybridisation analyses

Cells were cultured in 10 cm dishes in 10 ml of 1640 medium supplement with 10% FBS. After 24 hours, 100 μl of colcemid (10 μg/ml, Life Technologies, Carlsbad, CA) was added to each culture, and culture replaced to incubator for another one hour before harvesting. Cell suspension

bioRxiv preprint doi: https://doi.org/10.1101/504837; this version posted December 25, 2018. The copyright holder for this preprint (which was not certified by peer review) is the author/funder, who has granted bioRxiv a license to display the preprint in perpetuity. It is made available under aCC-BY-ND 4.0 International license.

was transferred to 15 ml cortical tubes. Culture medium was removed by centrifuge at 1000 rpm for 5 min. Cell pellet was subjected to hypotonic treatment with 0.075M KCl and then fixed with Methanol and acidic acid at 3:1v/v. Cell suspension is dropped to slides, and treated with 0.005% (wt/vol) pepsin solution for 10 min, followed by dehydration with 70%, 85%, and 100% (vol/vol) ethanol for 2 min each. Hybridization was performed by adding 10 μl of ALK dual color break apart probe on each slide (Cytocell, Cambridge UK), a coverslip was placed, and the slides were sealed with rubber cement. The specimens were subjected to denaturation at 75°C for 3 min and hybridized at 37°C for 16 h. The slides were washed in 0.4x saline-sodium citrate at pH 7.2 and then counterstained with DAPI. Results were analyzed on a Leica DM 5500B fluorescent microscope. Cell images were captured in both interphase and metaphase cells.

RNAseq analysis

Following 48 hours of culturing in the absence of inhibitors (to minimize the impact of directly induced gene expression changes), RNA was isolated from erALK-TKI and parental H3122 cells using an RNAEasy Minikit (Qiagen). Reads were generated using an Illumina NextSeq 500 instrument. Alignment was achieved using HiSat2. Normalized reads were obtained from DeSeq2. Analysis was performed with genes with more than 25 reads in at least one sample and more than two fold change from ALK TKI naïve cells in at least one resistant line.

Nanostring assay

Following 48 hours of culturing in the absence of inhibitors (to minimize the impact of directly induced gene expression changes), RNA was isolated from erALK-TKI and parental H3122 cells using an RNAEasy Minikit (Qiagen). The nCounter GX Human Cancer Reference Kit was used to determine gene reads. Genes more than one standard deviation from and more than two fold different from mean parental in any sample were retained for further analysis. The $\log_2\left(\frac{\text{Reads}}{\text{Median(Reads Across All Samples)}}\right)$ was used for all visualizations of the data. ClustVis [49] was used to generate PCA plots. Heatmap and corresponding dendograms were generated with heatmap.2 in R, using default parameters.

Single cell transcriptome analysis

Single cell expression was performed using 10x Genomics platform. 1000 cells were analyzed per each sample, and 40,000 reads per cell were generated using an Illumina NextSeq 500 instrument. Demultiplexing, barcode processing, alignment, gene counting and tSNE plot generation were performed using the 10X Genomics CellRanger 2.0 software. Violinplots of gene expression levels were generated using ggplot2 [50] in R and using default parameters, except adjust=2.

Immunoblots

Protein expression was analyzed using NuPAGE gels (ThermoFisher), following manufacturer's protocols. The following antibodies, purchased from Cell Signaling, were used: HER2 (4290), EGFR (2963), p-ALK Y1604 (3341), ALK (3633), p-Akt S473 (4060S), Akt (9272), pERK T202/T204 (4370S), ERK (4695), p-Stat3 Y705 (9145), Stat3 (9139), p-S6 S235/S236 (4858S) and s6 (2317). Anti- β-actin antibody was purchased from Santa Cruz (47778) and used at a 1:20,000 concentration. Secondary antibodies with H+L HRP conjugates were purchased from BioRad (anti-rabbit: 170-6515, anti-mouse:170-6516). HRP chemiluminescent substrate was purchased from Millipore (WBKLS0500). Images were taken using an Amersham Imager 600 (GE Healthcare Life Sciences).

bioRxiv preprint doi: https://doi.org/10.1101/504837; this version posted December 25, 2018. The copyright holder for this preprint (which was not certified by peer review) is the author/funder, who has granted bioRxiv a license to display the preprint in perpetuity. It is made available under aCC-BY-ND 4.0 International license.

Xenografts studies

erALK-TKI or parental H3122 were suspended in 1:1 RPMI/Matrigel (ThermoFisher) mix and subcutaneously implanted into 4-6 week-old NSG mice, with two contralateral injections per animal, containing 10^6 tumor cells each. After 3 weeks, the animals were treated with 25mg/kg alectinib (purchased from Astatech), 6mg/kg lorlatinib (obtained from Pfizer) or vehicle control via daily oral gavage. Tumor diameters were measured weekly using electronic calipers, and tumor volumes were calculated assuming spherical shape of tumors. For the first week of the collateral sensitivity experiment 11mg/kg alectinib was used. Xenograft studies were performed in accordance with the guidelines of the IACUC of the H. Lee Moffitt Cancer Center.

CRISPR Knockout experiments

To produce gRNA the following DNA oligos purchased from IDT were cloned into pSpCas9(BB)-2A-Puro (PX459) V2.0 vector (Addgene Plasmid #62988), using the protocol in [51]): CAC CGT CTC TCG GAG GAA GGA CTT G with AAA CCA AGT CCT TCC TCC GAG AGA C and CAC CGC ATC CTG CTG GAG CTC ATG G with AAA CCC ATG AGC TCC AGC AGG ATG C. H3122 cells were transfected with the above constructs using jetPrime reagent (polyPlus). 48 hours following transduction, 10^5 cells were seeded into per 6 cm dish for clonogenic assay. To account for differences in transfection efficiency between parental and resistant cell lines, control transfections were performed using MIG GFP expressing plasmid and analyzed for percentage of GFP expressing cells using flow cytometry. Normalization was performed by multiplying number of colonies by transfection coefficient (ratio between fraction of GFP + cells in GFP control transfection between a given cell line and parental cells).

cDNA expression

Entry cDNA ORFs in pDONOR223 or pENTR221 were obtained from human ORFeome collection v5.1 or Life Technologies, respectively. Lentiviral expression constructs were generated by Gateway swap into pLenti6.3/V5-Dest vector (Life Technologies). Oncogenic fusion gene EML4-ALK variant 1 wild type or point mutant at L1196M was cloned into the retroviral pBabe-puro backbone [31] (provided by J. Heuckmann, Universität zu Köln, Köln, Germany). Lentiviral and retroviral particles were produced, and used for transduction of H3122 cells following standard protocols, described in `https://www.addgene.org/protocols/lentivirus-production/` and `https://www.addgene.org/viral-vectors/retrovirus/retro-guide/`.

Acknowledgements

We thank M. Janiszewska, A. Goldman and A. Rozhok, for their critical reading of this manuscript and discussions, We thank I. Raplee for assistance with the RNASeq pipeline. We acknowledge members of Moffitt Molecular Genomics shared resource for technical assistance. The work was partially supported by Moffitt Lung Cancer Center of Excellence and NIH (U54 administrative supplement 10-18279-04-13); DLP was partially funded by IMFAHE travel fellowship.

bioRxiv preprint doi: https://doi.org/10.1101/504837; this version posted December 25, 2018. The copyright holder for this preprint (which was not certified by peer review) is the author/funder, who has granted bioRxiv a license to display the preprint in perpetuity. It is made available under aCC-BY-ND 4.0 International license.

References

[1] Sasaki, T., Rodig, S. J., Chirieac, L. R. & Jänne, P. A. The biology and treatment of EML4-ALK non-small cell lung cancer. *European Journal of Cancer* **46**, 1773–1780 (2010).

[2] Chmielecki, J. *et al.* Optimization of dosing for EGFR-mutant non–small cell lung cancer with evolutionary cancer modeling. *Science Translational Medicine* **3**, 90ra59–90ra59 (2011).

[3] Zhao, B. *et al.* Exploiting temporal collateral sensitivity in tumor clonal evolution. *Cell* **165**, 234–246 (2016).

[4] Gatenby, R. A., Silva, A. S., Gillies, R. J. & Frieden, B. R. Adaptive therapy. *Cancer research* **69**, 4894–4903 (2009).

[5] Goldman, A. *et al.* Temporally sequenced anticancer drugs overcome adaptive resistance by targeting a vulnerable chemotherapy-induced phenotypic transition. *Nature Communications* **6**, 6139 (2015).

[6] Zhang, J., Cunningham, J. J., Brown, J. S. & Gatenby, R. A. Integrating evolutionary dynamics into treatment of metastatic castrate-resistant prostate cancer. *Nature Communications* **8**, 1816 (2017).

[7] Burrell, R. A. & Swanton, C. Tumour heterogeneity and the evolution of polyclonal drug resistance. *Molecular Oncology* **8**, 1095–1111 (2014).

[8] Merlo, L. M., Pepper, J. W., Reid, B. J. & Maley, C. C. Cancer as an evolutionary and ecological process. *Nature Reviews Cancer* **6**, 924 (2006).

[9] Sharma, S. V. *et al.* A chromatin-mediated reversible drug-tolerant state in cancer cell subpopulations. *Cell* **141**, 69–80 (2010).

[10] Singh, A. & Settleman, J. EMT, cancer stem cells and drug resistance: an emerging axis of evil in the war on cancer. *Oncogene* **29**, 4741 (2010).

[11] Dhawan, A. *et al.* Collateral sensitivity networks reveal evolutionary instability and novel treatment strategies in ALK mutated non-small cell lung cancer. *Scientific Reports* **7**, 1232 (2017).

[12] McDermott, M. *et al.* In vitro development of chemotherapy and targeted therapy drug-resistant cancer cell lines: a practical guide with case studies. *Frontiers in Oncology* **4**, 40 (2014).

[13] Thakur, M. D. *et al.* Modelling vemurafenib resistance in melanoma reveals a strategy to forestall drug resistance. *Nature* **494**, 251 (2013).

[14] Moriceau, G. *et al.* Tunable-combinatorial mechanisms of acquired resistance limit the efficacy of BRAF/MEK cotargeting but result in melanoma drug addiction. *Cancer Cell* **27**, 240–256 (2015).

[15] Sieber, O. M., Tomlinson, S. R. & Tomlinson, I. P. Tissue, cell and stage specificity of (epi) mutations in cancers. *Nature Reviews Cancer* **5**, 649 (2005).

bioRxiv preprint doi: https://doi.org/10.1101/504837; this version posted December 25, 2018. The copyright holder for this preprint (which was not certified by peer review) is the author/funder, who has granted bioRxiv a license to display the preprint in perpetuity. It is made available under aCC-BY-ND 4.0 International license.

[16] Schneider, G., Schmidt-Supprian, M., Rad, R. & Saur, D. Tissue-specific tumorigenesis: context matters. *Nature Reviews Cancer* **17**, 239 (2017).

[17] Kaznatcheev, A., Peacock, J., Basanta, D., Marusyk, A. & Scott, J. G. Fibroblasts and Alectinib switch the evolutionary games played by non-small cell lung cancer. *Nature Ecology and Evolution* To appear (2018).

[18] Marusyk, A. *et al.* Non-cell-autonomous driving of tumour growth supports sub-clonal heterogeneity. *Nature* **514**, 54 (2014).

[19] Greaves, M. & Maley, C. C. Clonal evolution in cancer. *Nature* **481**, 306 (2012).

[20] Lewis, K. Persister cells, dormancy and infectious disease. *Nature Reviews Microbiology* **5**, 48 (2007).

[21] Balaban, N. Q., Merrin, J., Chait, R., Kowalik, L. & Leibler, S. Bacterial persistence as a phenotypic switch. *Science* **305**, 1622–1625 (2004).

[22] Hangauer, M. J. *et al.* Drug-tolerant persister cancer cells are vulnerable to GPX4 inhibition. *Nature* **551**, 247 (2017).

[23] Shaffer, S. M. *et al.* Rare cell variability and drug-induced reprogramming as a mode of cancer drug resistance. *Nature* **546**, 431 (2017).

[24] Rambow, F. *et al.* Toward minimal residual disease-directed therapy in melanoma. *Cell* **174**, 843–855 (2018).

[25] Hyo-eun, C. B. *et al.* Studying clonal dynamics in response to cancer therapy using high-complexity barcoding. *Nature Medicine* **21**, 440 (2015).

[26] Foo, J. & Michor, F. Evolution of acquired resistance to anti-cancer therapy. *Journal of Theoretical Biology* **355**, 10–20 (2014).

[27] Gainor, J. F. *et al.* Molecular mechanisms of resistance to first-and second-generation ALK inhibitors in ALK-rearranged lung cancer. *Cancer Discovery* CD–16 (2016).

[28] Nathanson, D. A. *et al.* Targeted therapy resistance mediated by dynamic regulation of extrachromosomal mutant EGFR DNA. *Science* **343**, 72–76 (2014).

[29] Mancini, M. & Yarden, Y. Mutational and network level mechanisms underlying resistance to anti-cancer kinase inhibitors. In *Seminars in Cell & Developmental Biology*, vol. 50, 164–176 (Elsevier, 2016).

[30] Zou, H. Y. *et al.* PF-06463922, an ALK/ROS1 inhibitor, overcomes resistance to first and second generation ALK inhibitors in preclinical models. *Cancer Cell* **28**, 70–81 (2015).

[31] Zhang, G. *et al.* Coupling an EML4-ALK–centric interactome with RNA interference identifies sensitizers to ALK inhibitors. *Sci. Signal.* **9**, rs12–rs12 (2016).

[32] Katayama, R. *et al.* Therapeutic strategies to overcome crizotinib resistance in non-small cell lung cancers harboring the fusion oncogene EML4-ALK. *Proceedings of the National Academy of Sciences* **108**, 7535–7540 (2011).

bioRxiv preprint doi: https://doi.org/10.1101/504837; this version posted December 25, 2018. The copyright holder for this preprint (which was not certified by peer review) is the author/funder, who has granted bioRxiv a license to display the preprint in perpetuity. It is made available under aCC-BY-ND 4.0 International license.

[33] Paasinen-Sohns, A. *et al.* Single-center experience with a targeted next generation sequencing assay for assessment of relevant somatic alterations in solid tumors. *Neoplasia* **19**, 196–206 (2017).

[34] Weinberg, R. *The biology of cancer* (Garland science, 2013).

[35] Burrell, R. A., McGranahan, N., Bartek, J. & Swanton, C. The causes and consequences of genetic heterogeneity in cancer evolution. *Nature* **501**, 338 (2013).

[36] Cahill, D. P., Kinzler, K. W., Vogelstein, B. & Lengauer, C. Genetic instability and darwinian selection in tumours. *Trends in Cell Biology* **9**, M57–M60 (1999).

[37] Mayr, E. *The growth of biological thought: Diversity, evolution, and inheritance* (Harvard University Press, 1982).

[38] Marusyk, A. Obstacles to the darwinian framework of somatic cancer evolution. In *Ecology and Evolution of Cancer*, 223–227 (Elsevier, 2017).

[39] Feinberg, A. P. Phenotypic plasticity and the epigenetics of human disease. *Nature* **447**, 433 (2007).

[40] Pisco, A. O. & Huang, S. Non-genetic cancer cell plasticity and therapy-induced stemness in tumour relapse:'What does not kill me strengthens me'. *British Journal of Cancer* **112**, 1725 (2015).

[41] Roe, J.-S. *et al.* Enhancer reprogramming promotes pancreatic cancer metastasis. *Cell* **170**, 875–888 (2017).

[42] Kim, C. *et al.* Chemoresistance Evolution in Triple-Negative Breast Cancer Delineated by Single-Cell Sequencing. *Cell* **173**, 879–893 (2018).

[43] Salgia, R. & Kulkarni, P. The genetic/non-genetic duality of drug 'resistance' in cancer. *Trends in Cancer* (2018).

[44] Marusyk, A., Almendro, V. & Polyak, K. Intra-tumour heterogeneity: a looking glass for cancer? *Nature Reviews Cancer* **12**, 323 (2012).

[45] Lee, M. J. *et al.* Sequential application of anticancer drugs enhances cell death by rewiring apoptotic signaling networks. *Cell* **149**, 780–794 (2012).

[46] Pisco, A. O. *et al.* Non-Darwinian dynamics in therapy-induced cancer drug resistance. *Nature Communications* **4**, 2467 (2013).

[47] Marusyk, A., Wheeler, L. J., Mathews, C. K. & DeGregori, J. p53 mediates senescence-like arrest induced by chronic replicational stress. *Molecular and Cellular Biology* **27**, 5336–5351 (2007).

[48] Wei, T. & Simko, V. corrplot: Visualization of a correlation matrix. *R package version 0.73* **230**, 11 (2013).

[49] Metsalu, T. & Vilo, J. ClustVis: a web tool for visualizing clustering of multivariate data using Principal Component Analysis and heatmap. *Nucleic Acids Research* **43**, W566–W570 (2015).

bioRxiv preprint doi: https://doi.org/10.1101/504837; this version posted December 25, 2018. The copyright holder for this preprint (which was not certified by peer review) is the author/funder, who has granted bioRxiv a license to display the preprint in perpetuity. It is made available under aCC-BY-ND 4.0 International license.

[50] Wickham, H. *ggplot2: elegant graphics for data analysis* (Springer, 2016).

[51] Bauer, D. E., Canver, M. C. & Orkin, S. H. Generation of genomic deletions in mammalian cell lines via CRISPR/Cas9. *Journal of Visualized Experiments: JoVE* (2015).